

# NEXAFS characterization of DNA components and molecular-orientation of surface-bound DNA oligomers

Newton T. Samuel<sup>a</sup>, Chi-Ying Lee<sup>a</sup>, Lara J. Gamble<sup>b</sup>, Daniel A. Fischer<sup>c</sup>, David G. Castner<sup>a,b,\*</sup>

<sup>a</sup> National ESCA and Surface Analysis Center for Biomedical Problems, Department of Chemical Engineering, University of Washington, Box 351750, Seattle, WA 98195, United States

<sup>b</sup> National ESCA and Surface Analysis Center for Biomedical Problems, Department of Bioengineering, University of Washington, Box 351750, Seattle, WA 98195, United States

<sup>c</sup> National Institute of Standards and Technology, Gaithersburg, MD 20899, United States

Received 29 August 2005; received in revised form 14 April 2006; accepted 14 April 2006

Available online 2 May 2006

## Abstract

Single stranded DNA oligomers (ssDNA) immobilized onto solid surfaces forms the basis for several biotechnological applications such as DNA microarrays, affinity separations, and biosensors. The surface structure of the surface-bound oligomers is expected to significantly influence their biological activity and interactions with the environment. In this study near-edge X-ray absorption fine structure spectroscopy (NEXAFS) is used to characterize the components of DNA (nucleobases, nucleotides and nucleosides) and the orientation information of surface-bound ssDNA. The K-edges of carbon, nitrogen and oxygen have spectra with features that are characteristic of the different chemical species present in the nucleobases of DNA. The effect of addition of the DNA sugar and phosphate components on the NEXAFS K-edge spectra was also investigated. The polarization-dependent nitrogen K-edge NEXAFS data show significant changes for different orientations of surface bound ssDNA. These results establish NEXAFS as a powerful technique for chemical and structural characterization of surface-bound DNA oligomers.

© 2006 Elsevier B.V. All rights reserved.

**Keywords:** NEXAFS; XPS; DNA; Monolayers

## 1. Introduction

Immobilization of single-stranded DNA oligomers (ssDNA) onto solid surfaces and characterizing their molecular organization on the surface (packing density, orientation, etc.) is of significant importance for applications such as diagnostics, DNA microarrays, etc. [1–12]. There are several different schemes that have been used to immobilize ssDNA onto a surface [13–21]. These different approaches can cause the ssDNA molecules to be immobilized onto the surface with different surface structures. For example, DNA physically immobilized onto poly(lysine) coated surfaces would be expected to lie flat on the surface due to strong interaction between the negatively charged phosphate backbone and the positively charged lysine groups [22]. Specific immobilization through thiol linkers attached to their 3' or 5' ends of the DNA oligomer is expected to result in a more

upright orientation [23–29]. The different orientations resulting from the different immobilization methods could have significant influence on the hybridization efficiency of ssDNA. Hence, information about the structure of immobilized ssDNA would be invaluable for optimizing the performance of DNA microarrays and other applications using surface-bound oligomers.

Various tools have been employed to characterize the immobilization of ssDNA to gold surfaces with a short alkanethiol linker and the subsequent hybridization with complement DNA. These tools include X-ray Photoelectron Spectroscopy (XPS) [14,30], radiolabeling [14], neutron reflectivity [31], Surface Plasmon Resonance (SPR) [23], Atomic Force Microscopy (AFM) [32], and more recently FT-IR [24]. The results from these characterization experiments have provided information about the structure of surface immobilized ssDNA. Based on XPS [14,30], neutron reflectivity [31] and electrophoretic measurement [26], thiolated ssDNA has been proposed to initially bind to the surface through the nitrogen groups in the bases, then become more upright when backfilled with short-chain alkyl thiol molecules.

\* Corresponding author. Tel.: +1 206 543 8094; fax: +1 206 543 3778.  
E-mail address: [castner@nb.engr.washington.edu](mailto:castner@nb.engr.washington.edu) (D.G. Castner).

The first part of the paper describes the near-edge structure at the carbon, nitrogen and oxygen K-edges of the different DNA components (nucleobases, nucleotides and nucleosides). The present study extends the earlier experiments [33–37] characterizing the near-edge structure of the DNA bases by systematically examining the effect observed in the NEXAFS spectra when DNA sugar and phosphate groups are added to the nucleobases. All the samples were prepared by the same procedure used in a previous Time-of-Flight Secondary Ion Mass Spectrometry (ToF-SIMS) and XPS study [38]. The latter part of the paper demonstrates the ability to probe different molecular orientations of the surface immobilized ssDNA. The ability to obtain information about molecular orientation is demonstrated by using ssDNA sequences that adopt different orientations on the surface.

## 2. Experimental methods

### 2.1. Preparation of the reference samples

Nucleobases (adenine, cytosine, guanine, thymine, uracil), nucleosides – nucleobase plus one sugar – (2'-deoxyadenosine, 2'-deoxycytidine, 2'-deoxyguanosine, thymidine, 2'-deoxyuridine) and the nucleotides – base plus sugar plus phosphate – (2'-deoxyadenosine 5'-monophosphate, 2'-deoxycytidine 5'-monophosphate, 2'-deoxyguanosine 5'-monophosphate, thymidine 5'-monophosphate and 2'-deoxyuridine 5'-monophosphate) were purchased from Sigma Chemical (St. Louis, MO) and were used as received. Indium shot was obtained from AESAR (Seabrook, NH). Small pieces of Indium shot (~2 mm radius) were cut with a scalpel to expose fresh metal surfaces, then pressed into disks of ~5 mm radius. The DNA powders were compacted into the surface of the indium disks. Because of the pliable nature of indium, the powders were easily compacted into the metal and provide a stable and smooth surface for analysis. All the samples were stored under nitrogen in Petri dishes until analysis.

### 2.2. Gold substrate preparation

Gold-coated silicon wafers were used as substrate material for DNA immobilization. Silicon wafers (Silicon Valley Microelectronics, Inc., San Jose) were diced into 10 mm × 10 mm squares and cleaned by sonication in DI water, methylene chloride, acetone, and methanol for 5 min two times in each solvent. Substrates were coated by electron beam evaporation of a 10 nm titanium adhesive layer followed by a 100 nm gold layer (99.99%) at pressures below  $1 \times 10^{-6}$  Torr.

### 2.3. Adsorption of the DNA oligomers

The HPLC purified synthetic ssDNA oligomers were obtained from Trilink Biotechnologies [39]. All the oligos were stored in 25 mM Tris at pH 7.4. The sequences for the different oligomers were:

- polydT-SH: 5'-HS-(CH<sub>2</sub>)<sub>6</sub>-(dT)<sub>16</sub>-3'
- polydA: 5'-(dA)<sub>16</sub>-3'

where dA = deoxyadenosine and dT = deoxythymidine.

The adsorption experiments were done at room temperature from 1 μM solutions in TE buffer (10 mM Tris, 1 mM EDTA and 1 M NaCl at pH 7.0) for time periods up to 24 h. The samples were then washed copiously with DI water (resistivity > 18 MΩ cm) and stored in Petri dishes and back-filled with nitrogen until analysis.

### 2.4. X-ray photoelectron spectroscopy

All XPS data were acquired on a Surface Science Instruments S-probe spectrometer. This instrument has a monochromatized Al Kα X-ray source, hemispherical analyzer, multi-channel detector and a low energy electron flood gun for charge neutralization. X-ray spot size for these acquisitions was 800 μm × 800 μm. Pressure in the analytical chamber during spectral acquisition was less than  $5 \times 10^{-9}$  Torr. The analyzer pass energy for the survey spectra (composition) was 150 eV and for high resolution C1s spectra was 50 eV. The take-off angle (the angle between the sample normal and the input axis of the analyzer lens) was 55° (a 55° take-off angle corresponds to a ~50 Å sampling depth). The Service Physics ESCAVB Graphics Viewer program was used to determine peak areas, to calculate the elemental compositions from peak areas, and to peak fit the high resolution spectra.

### 2.5. Near-edge X-ray absorption fine structure (NEXAFS)

The NEXAFS experiments were done at the National Synchrotron Light Source (NSLS), NIST U7-A beamline. The beamline uses a ~85% polarized, high intensity beam and a monochromator with 600 l/mm grating that provides a full-width at half-maximum (FWHM) resolution of ~0.15 eV at the carbon K-edge. The monochromator energy scale was calibrated by setting the C (1s) to  $\pi^*$  transition in the graphite carbon K-edge NEXAFS spectrum to 285.35 eV [40]. Partial electron yield (PEY) was monitored using a channeltron with a negatively applied bias voltage to monitor the Auger and photoelectron yield from the sample. The NEXAFS spectra were normalized with the signal ( $I_0$ ) from an in situ gold coated 90% transmission grid placed in the path of the X-rays, to account for changes in the incoming X-ray intensity with time and energy changes.

The data for the reference bases was collected with the channeltron cone bias voltage maintained at –150 V for the carbon K-edge spectrum, –280 V for the nitrogen K-edge spectrum and –390 V for the oxygen K-edge spectrum. The higher bias voltages for the nitrogen and the oxygen K-edges were used to eliminate the carbon and nitrogen Auger electrons. For all the spectra, the pre-edge was subtracted using a linear background and then normalized to unit absorption jump height. The reference spectra of the different nucleobases, nucleosides and nucleotides were acquired at an angle of 55° where the polarization effects were expected to be minimal. An electron flood

gun operating in constant current mode with electron energy of 10 eV and an emission current of 60  $\mu\text{A}$  was employed to prevent charging of the substrates.

The nitrogen K-edge spectra for polydT-SH and polydA were collected with a detector bias voltage of  $-360$  V. This removed the carbon Auger signal and the Au 4d photoelectrons, and resulting in a more straightforward background subtraction of the partial electron yield data in the nitrogen K-edge region. A small dip was detected around 427 eV due to the second harmonic peak of the nickel line. The presence of the nickel likely arises from contamination in the beamline optics and is detected only when the detector bias is around  $-360$  V. For lower values of the grid bias, a higher electron yield signal is obtained, and this feature is no longer prominent. Polarization-dependent experiments to probe the orientation of the immobilized ssDNA were done by monitoring the NEXAFS spectra at various polar angles (the angle between the incoming X-rays and the sample surface). At normal incidence the direction of the incoming X-rays is normal to the sample surface and at glancing incidence the incoming X-rays are  $20^\circ$  from the sample surface. The pre-edge was first subtracted from the spectra using a linear background. Then the difference in the signal 40 eV above and below the first resonance was normalized to unit absorption jump height. A disordered system does not show any polarization-dependence (change in NEXAFS peak intensities with changing incidence angle of the X-rays) because of random distribution of the molecular orientations. However, as the directional alignment of the molecules in the overlayer increases the polarization-dependence of the NEXAFS spectra will increase.

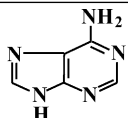
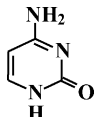
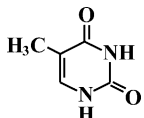
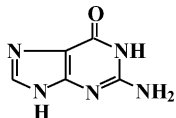
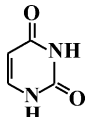
The possible effect of X-ray irradiation on the ssDNA oligomers was examined by repeated exposure to X-rays. No significant changes in the nitrogen K-edge spectra were observed in repeated scans, indicating the ssDNA samples were stable under the X-ray flux used to acquire the NEXAFS spectra (data not shown). This is unlike peptides and proteins, which show additional beam damage features in the nitrogen K-edge spectra in repeated scans [41].

### 3. Results and discussion

#### 3.1. Carbon K-edge of the DNA bases

The structures of the different DNA nucleobases are shown in Table 1. The carbon K-edge NEXAFS spectra of these nucleobases are shown in Fig. 1. As can be seen from the spectra in Fig. 1, the different nucleobases could be distinguished based on their characteristic carbon K-edge spectra (except thymine and uracil, which only differ by replacement of a hydrogen atom in uracil with a methyl group in thymine). The peak positions for the  $\pi^*$  orbitals for the nucleobases are listed in Table 2. Using results from previous studies on amino acids and polymers [33–37,42–48], the major peaks in the spectrum of thymine and uracil can be uniquely assigned to the functional groups present in these nucleobases. For example, the peak at 288.1 eV is assigned to a transition to the  $\pi^*$  orbital of the  $\text{O}=\text{C}-\text{NH}$  group ( $\pi_{\text{CONH}}^*$ ). This assignment is based on the work done recently showing how the  $\pi_{\text{CO}}^*$  peak shifts with addition of different

Table 1  
Chemical structures of the DNA nucleobases

Adenine (A)	
Cytosine (C)	
Thymine (T)	
Guanosine (G)	
Uracil (U)	

groups [48]. The  $\pi_{\text{CO}}^*$  peak normally appears at 286.6 eV, but is shifted to 288.1 eV when a nitrogen is attached to the carbonyl group. Similarly, the peak shifts further to 289.4 eV when two nitrogens are attached to the carbonyl group. Thus, the peak at 289.4 eV in the thymine and uracil spectra can be assigned to the  $\pi_{\text{HNCONH}}^*$  peak. The peak at 285 eV is assigned to  $\pi_{\text{C}=\text{C}}^*$  species, similar to the features found in NEXAFS spectra of polymers

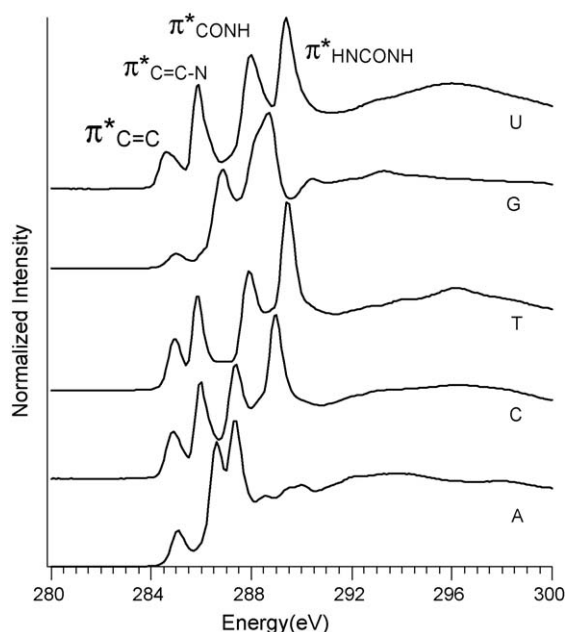


Fig. 1. Carbon K-edge NEXAFS spectra of the DNA nucleobases.

Table 2

Peak positions of the prominent  $\pi^*$  features in the carbon K-edge NEXAFS spectra for DNA nucleobases and nucleosides

	$\pi_1^*$ (eV)	$\pi_2^*$ (eV)	$\pi_3^*$ (eV)	$\pi_4^*$ (eV)	$\pi_5^*$ (eV)
A	285.1	286.5	287.5	–	–
C	284.9	286.0	287.5	–	288.9
T	284.9	285.8	288.0	–	289.4
G	285.0	286.5	288.1	–	288.6
U	284.8	285.9	288.0	–	289.4
A+S	285.0	286.6	287.5	288.5	–
C+S	284.9	285.9	287.4	288.4	289.0
T+S	284.9	285.7	287.9	288.5	289.4
G+S	285.0	286.8	287.4	288.1	288.6
U+S	284.8	285.9	288.0	288.5	289.4

A = adenine, T = thymine, C = cytosine, G = guanine, U = uracil, S = sugar, and P = phosphate group.

[49] and amino acids [46] containing double-bonded and aromatic carbon atoms. The peak at 286 eV is assigned to a  $\pi_{\text{C}=\text{C}-\text{N}}^*$  species based on the assignments for the amino acids [46]. This building block approach to interpreting the peaks found in the NEXAFS spectra is successful in explaining the many features in NEXAFS spectra, provided there is not extensive delocalization in the structure resulting in new electronic states [49]. The spectra of polymers and amino acids have been explained using the building block approach [43,45,46,49].

Adenine has a double ring structure that contains carbon, nitrogen and hydrogen atoms. A small  $\pi_{\text{C}=\text{C}}^*$  peak is observed at 285 eV. The two strong peaks near 286.5 and 287.5 are from the  $\text{C}-\text{N}_x$  species in the adenine structure. Guanosine has a similar two ring structure to adenine. The two differences between these nucleobases is the location of the amine group on the six-member ring and the addition of a carbonyl group in guanosine (see Table 1). These changes do not change the location of the  $\text{C}-\text{N}$  peak at 286.5 in the guanosine spectrum, but does result in an unresolved doublet near 288.5 eV. Part of the intensity of this doublet is due to a  $\pi_{\text{CONH}}^*$  peak. The structure of cytosine is similar to that of uracil. The only difference is one of the carbonyl groups in uracil have been replaced by an amine group in cytosine (see Table 1). This replacement does not change the energies of the  $\pi_{\text{C}=\text{C}}^*$  and  $\pi_{\text{C}=\text{C}-\text{N}}^*$  peaks, but does slightly lower the energy of the  $\pi_{\text{HCONH}}^*$  peak. The cytosine spectrum also has a peak near 287.5 eV. Based on the fact three nucleobases with amine groups attached to ring structures (adenine, cytosine, and guanosine) all have peaks in their NEXAFS spectrum near 287 eV is likely this peak is due to a transition to the  $\pi^*$  orbital of the  $\text{C}-\text{NH}_x$  group. However, because of the extended aromatic structure of adenine, cytosine and guanosine, rigorous quantum mechanical calculations are needed to confirm the peak assignments for their NEXAFS spectra. It has been recently shown that ab initio calculations are capable of capturing the different  $\pi^*$  features in NEXAFS spectra arising from different carbon species [34,42,47].

### 3.2. DNA bases nitrogen K-edge

The nitrogen in the DNA resides in the nucleobases. Hence, the nitrogen K-edge spectra can be used to selectively probe the

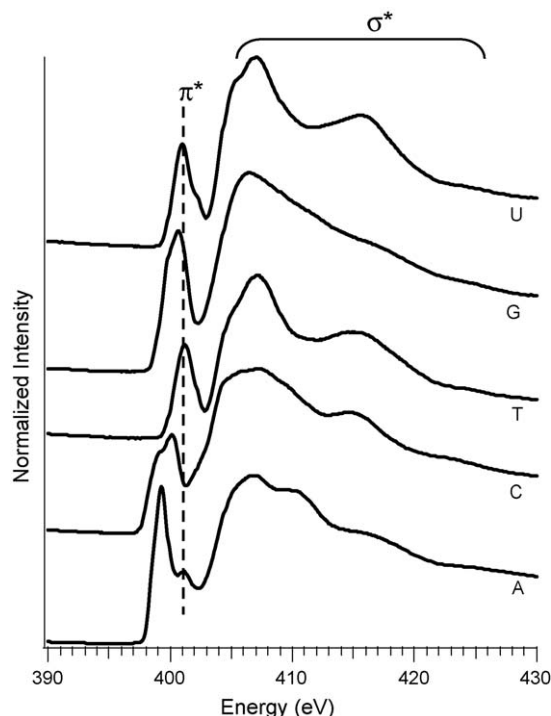


Fig. 2. Nitrogen K-edge NEXAFS spectra of the DNA nucleobases.

nucleobase structure in immobilized ssDNA. The nitrogen K-edge NEXAFS spectra shown in Fig. 2 for the five nucleobases can be divided into two regions. Peaks due to transitions to  $\pi^*$  orbitals are located around 400 eV and peaks due to transitions to  $\sigma^*$  orbitals are located above 405 eV. These assignments are based on recent quantum mechanical calculations and experimental studies [35,44]. The peak positions for the  $\pi^*$  orbitals for the nucleobases are listed in Table 3. Similar to the carbon K-edge spectra, the nitrogen K-edge spectra exhibit differences among the five nucleobases. The  $\pi^*$  peaks in thymine and uracil spectra are near 401 eV, consistent with the fact that all nitrogen atoms in these two nucleobases are located next to carbonyl groups. The major  $\pi^*$  peak for adenine, which has no carbonyl

Table 3

Peak positions of the prominent  $\pi^*$  features in the nitrogen K-edge NEXAFS spectra for DNA nucleobases, nucleotides, and nucleosides

	$\pi_1^*$ (eV)	$\pi_2^*$ (eV)
A	399.3	401.2
C	399.0	400.2
T	401.2	–
G	399.9	400.7
U	401.0	–
A+S	399.4	401.7
C+S	399.0	400.1
T+S	401.0	–
G+S	399.9	401.6
U+S	401.0	–
A+S+P	399.4	401.2
C+S+P	399.9	400.8
T+S+P	401.3	–
G+S+P	399.8	401.0
U+S+P	401.3	–

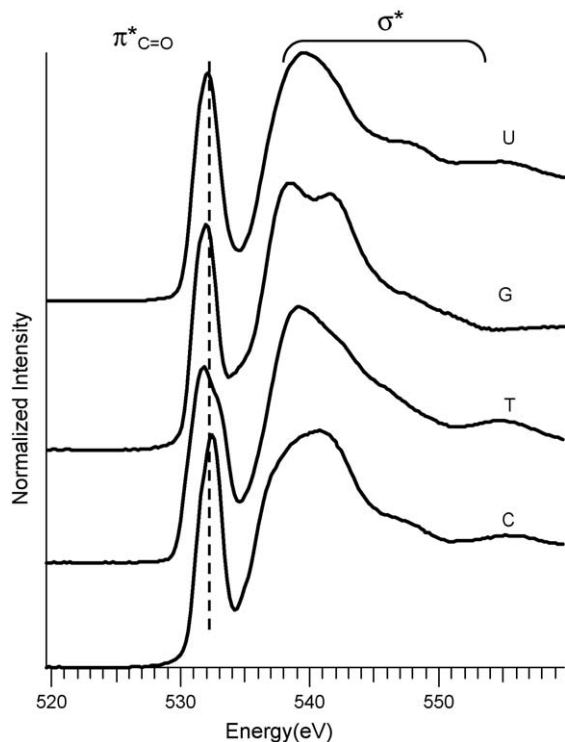


Fig. 3. Oxygen K-edge NEXAFS spectra of the DNA nucleobases.

groups, is located near 399 eV, consistent with the location of the nitrogen  $\pi^*$  peak in other biomolecules that have nitrogen atoms present in a ring structure (e.g., the amino acid histidine) [41,46,50]. The remaining two nucleobases, guanosine and cytosine, have nitrogen groups both adjacent and removed from carbonyl groups (see Table 1). These two nucleobases have unresolved doublet  $\pi^*$  peaks in the 399–401 eV energy range (see Table 3 for the exact energy positions), consistent with the type of nitrogen species in guanosine and cytosine.

### 3.3. DNA bases oxygen K-edge

The oxygen K-edge NEXAFS spectra of the five nucleobases are shown in Fig. 3. The peak positions for the  $\pi^*$  orbitals for the nucleobases are listed in Table 4. Recent quantum mechanical calculations have shown the  $\pi^*$  peak for carbonyl species ( $\pi^*_{C=O}$ ) is located near 532 eV and  $\sigma^*$  peaks for oxygen species are located above 535 eV [35]. The peak positions in Fig. 3 are consistent with these assignments. All nucleobases except adenine have a strong  $\pi^*_{C=O}$  peak near 532 eV and  $\sigma^*$  peaks above 535 eV. The relative intensities and positions of the  $\sigma^*$  peak vary slightly among the nucleobases, as expected from their slightly different structures. Thymine shows a slight splitting of the  $\pi^*_{CO}$  peak compared to the other nucleobases. Uracil does not show an apparent splitting of the  $\pi^*_{CO}$  because of the lower energy resolution at the oxygen K-edge. The position of the  $\pi^*_{CO}$  is shifted to 532.5 eV for cytosine. Similar trends have been reported earlier as well [35,48]. As expected NEXAFS spectra of adenine does not show any signal since it does not contain oxygen (data not shown).

Table 4

Peak positions of the prominent  $\pi^*$  features in the oxygen K-edge NEXAFS spectra for DNA nucleobases, nucleosides and nucleotides

	$\pi^*_1$ (eV)	$\pi^*_2$ (eV)
A	–	–
C	532.5	–
T	531.8	533.0
G	531.8	–
U	532.1	–
A+S	–	–
C+S	532.5	–
T+S	531.9	–
G+S	532.0	–
U+S	531.9	–
A+S+P	–	–
C+S+P	532.3	–
T+S+P	532.0	–
G+S+P	531.9	–
U+S+P	531.9	–

### 3.4. Effect of addition of different DNA constituents in their NEXAFS spectra

DNA is made up of the different nucleobases, each attached to a ribose sugar and a phosphate group (see insert in Fig. 4). Thymine is used as a typical case to show the effect on the carbon K-edge NEXAFS spectra of adding the sugar and phosphate groups (Fig. 4). The NEXAFS carbon K-edge spectra of the thymine nucleotide (thymidine 5'-monophosphate) were not collected because of excess carbon contamination in the sample (similar problems were observed with the XPS characterization results [38]). For this reason, the spectrum of polydT-SH

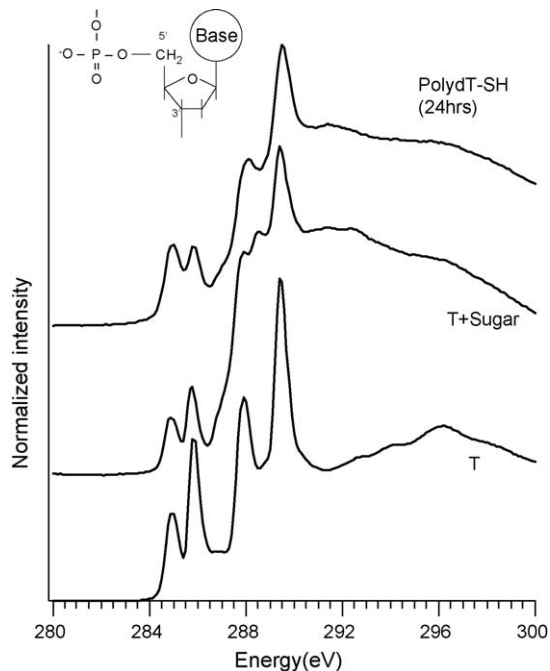


Fig. 4. The effect on the carbon K-edge NEXAFS spectra from adding the sugar and phosphate groups of DNA to thymine (T). The insert shows a schematic that represents the chemical structure of DNA with its nucleobase, sugar and phosphate components.

(24 h) is used to represent the effect of addition of the phosphate group. The major peaks expected from the thymine  $\pi^*$  features are present in all three spectra, but their intensities vary as the sugar and phosphate groups are added. With the addition of the sugar to the base, a new peak at 288.5 eV is observed, which is attributed to the  $\sigma^*$  peak from the carbon atoms attached to the oxygen in the sugar unit [49,51]. Upon addition of the sugar, enhanced intensities are also seen in the  $\sigma^*$  peaks from the C–C and the C–O bonds in the region beyond 290 eV. PolydT-SH shows a similar spectrum to the thymine nucleoside spectrum. This is expected since the phosphate group does not contain any carbon atoms. Similar trends were seen for the other nucleobases upon addition of the sugar in the carbon K-edge region (data not shown). The increase in intensity of the  $\pi^*$  feature at 285 eV for PolydT-SH is due to adventitious carbon contamination. This is evident from the excess carbon seen in the XPS composition data for PolydT-SH (Table 6).

Using guanine as a typical example, the effect of adding the sugar and phosphate groups to a nucleobase on nitrogen K-edge NEXAFS spectra is shown in Fig. 5. Since neither the sugar or phosphate groups contain nitrogen, no large changes are expected. This is the case for the  $\sigma^*$  region above 405 eV. However, the addition of sugar and the phosphate groups did have a noticeable effect in the  $\pi^*$  region of the spectrum. This effect is most apparent for guanine, which shows shifts in the position of the  $\pi^*$  peaks (see Table 3). However, detailed calculations are needed to understand the origin of the shift in the  $\pi^*$

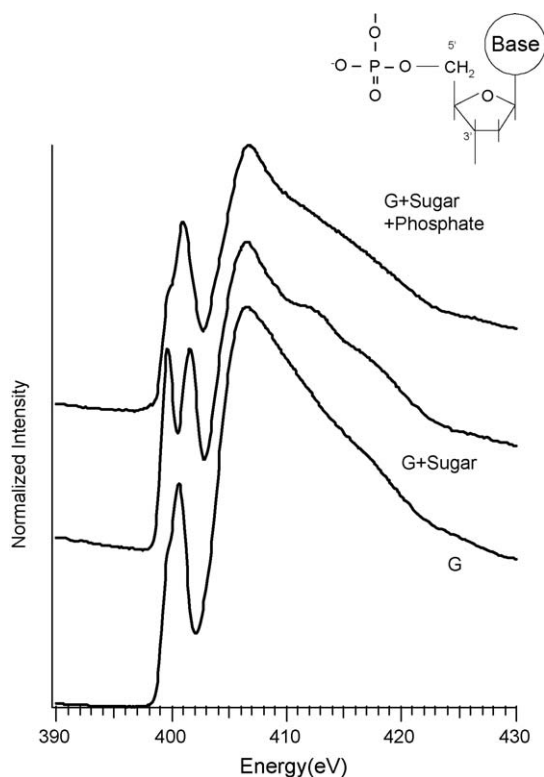


Fig. 5. The effect on the nitrogen K-edge NEXAFS spectra from adding the sugar and phosphate groups of DNA to guanine (G). The insert shows a schematic that represents the chemical structure of DNA with its nucleobase, sugar and phosphate components.

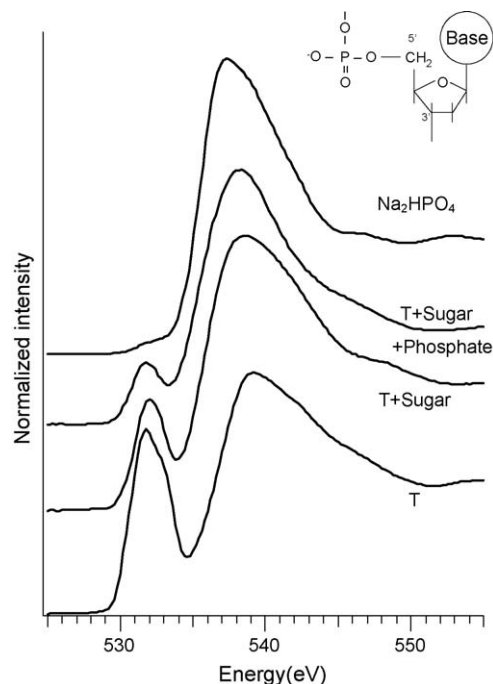


Fig. 6. The effect on the oxygen K-edge NEXAFS spectra from adding the sugar and phosphate groups of DNA to thymine (T). A reference spectrum of sodium phosphate is also shown. The insert shows a schematic that represents the chemical structure of DNA with its nucleobase, sugar and phosphate components.

peak positions. Adenine also shows some shifting in the position of the second  $\pi^*$  peak around 401.5 eV (see Table 3). Thymine and uracil do not show large changes in the position of their  $\pi^*$  peak with the addition of the sugar and phosphate groups (see Table 3).

The effect in the oxygen K-edge of adding the sugar and phosphate groups to thymine is shown in Fig. 6. The major change is a significant reduction in the  $\pi^*_{C=O}$  intensity relative to the  $\sigma^*$  intensities. This is expected since the oxygen species in the sugar and phosphate groups should only contribute intensity in the  $\sigma^*$  region. The spectrum of a sodium phosphate salt is shown to provide an example of the oxygen K-edge spectra of the phosphate group. With the addition of the sugar and phosphate groups, the thymine spectrum becomes more characteristic of the phosphate group.

### 3.5. Probing the molecular-orientation of surface-bound DNA oligomers

To determine the ability of NEXAFS to probe the orientation of surface-bound ssDNA two different oligomers which adopt different surface structures on gold surfaces were selected for investigation. The first was polydT-SH, which should attach to the surface through the thiol groups and is expected to adopt a more upright structure. The second was polydA, which should attach to the surface through interactions with nitrogen groups in the nucleobases and is expected to adopt a more flat orientation. Recent results from several studies point to the different molecular orientations adopted by specifically (through thiol) and non-specifically (through the side-chain bases) immobi-

Table 5  
Elemental composition (atomic percentage  $\pm$  standard deviation) determined by XPS for the ssDNA oligomers adsorbed onto gold surfaces from TE buffer at different adsorption times

	C 1s	N (1s)	O (1s)	P (2p)	S (2p)	Au (4f)
PolydT-SH (24 h)	46.8 $\pm$ 1.1	6.7 $\pm$ 1.0	24.8 $\pm$ 0.2	2.9 $\pm$ 0.6	0.0	18.8 $\pm$ 0.3
PolydA (24 h)	38.2 $\pm$ 5.5	8.0 $\pm$ 1.3	16.1 $\pm$ 1.4	0.0	0.0	37.7 $\pm$ 2.9

Table 6  
Theoretical vs. XPS-determined elemental compositions (atomic percentage  $\pm$  standard deviation) of the DNA oligomers excluding gold

	C 1s	N (1s)	O (1s)	P (2p)	S (2p)	P/N	C/N	O/N
PolydT-SH (24 h)	57.7 $\pm$ 1.2	8.2 $\pm$ 1.3	30.5 $\pm$ 0.3	3.6 $\pm$ 0.7	0.0	0.4	7.0	3.7
PolydT-SH (theoretical)	50.9	9.5	34.3	5.0	0.3	0.5	5.4	3.6
PolydA (24 h)	61.1 $\pm$ 5.9	12.9 $\pm$ 2.6	26.0 $\pm$ 3.4	0.0	0.0	0.0	5.0	2.0
PolydA (theoretical)	47.6	23.8	23.8	4.8	0.0	0.2	2.0	1.0

lized ssDNA oligomers [23–29,52]. In particular, polydA was immobilized non-specifically because of the amine groups in the nucleobases interacting with the gold surface [23,24]. In contrast, polydT-SH would be primarily immobilized through the thiol groups because of the low affinity of its nucleobases to the gold surface [24]. Hence, we hypothesize that the two immobilized ssDNA molecules on gold surfaces should exhibit different polarization-dependent NEXAFS spectra characteristic of their different interactions and structures on gold surfaces.

The elemental surface compositions of the different oligomers adsorbed onto gold surfaces are listed in Table 5. All the elements from the ssDNA oligomers are detected, except sulfur from polydT-SH. Sulfur is not detected because of its low concentration in polydT-SH (S atomic percent = 0.3%) and its attenuation by the immobilized ssDNA overlayer. The XPS determined P/N and O/N elemental ratios for polydT-SH agree well with the theoretical ratios expected from the stoichiometry of the polydT-SH (Table 6). The agreement between the XPS and theoretical P/N and O/N ratios is not as good for polydA. For both ssDNA oligomers the amount of carbon determined by XPS was greater than the amount expected from their stoichiometries (see Table 6), indicating the presence of some hydrocarbon contamination on these samples. The carbon concentration did decrease for polydT-SH at the 24 h assembly time relative to earlier time points (data not shown), indicating as more ssDNA oligomers are immobilized onto the surface some of the residual carbon contamination is removed from the gold surface. The XPS gold concentration for the 24 h assembly of polydT-SH was half the value of the gold concentration for the 24 h assembly of polydA. The differences in the gold concentrations indicate the polydT-SH overlayer was thicker or more dense than the polydA overlayer. This is consistent with a more upright surface-structure of polydT-SH on gold compared to polydA.

Fig. 7 shows the polarization-dependent nitrogen K-edge spectra of the two ssDNA oligomers immobilized onto gold. The  $\pi^*$  region of the polydT-SH spectrum exhibits enhanced intensity at glancing X-ray incidence. In contrast the  $\pi^*$  region of the polydA spectrum exhibits enhanced intensity at normal X-ray incidence. Since the electric field vector of the incident X-ray beam is parallel to the surface at normal incidence this

means on gold surfaces polydT-SH stands more upright structure with the plane of the nucleobases relatively parallel to the surface while polydA lies flat on the surface with the plane of the nucleobases relatively perpendicular to the surface (see the idealized schematic in Fig. 8). Similar trends were observed with surface-bound double-stranded DNA oligomers [53] and surface-bound single-stranded peptide nucleic acids [52,54,55] on gold surfaces. This result is also consistent with previous studies that show polydT-SH binds mostly through the thiol group and polydA binds mostly through the nucleobases [23–25]. However, the amount of polarization-dependence in the nitrogen K-edge spectra of both ssDNA samples is relatively small. This is suggestive of some disorder in the ssDNA monolayers

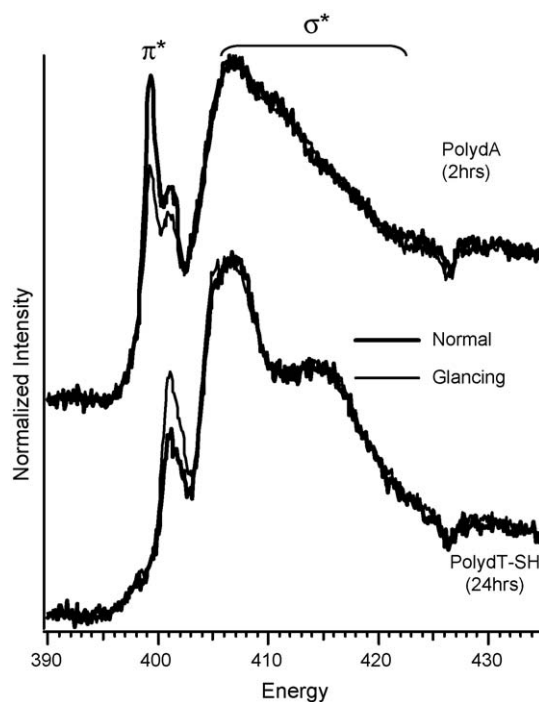


Fig. 7. Nitrogen K-edge NEXAFS spectra at normal and glancing X-ray incidence for ssDNA oligomers adsorbed onto gold surfaces. (a) PolydA (24 h adsorption time) and (b) PolydT-SH (24 h adsorption time).

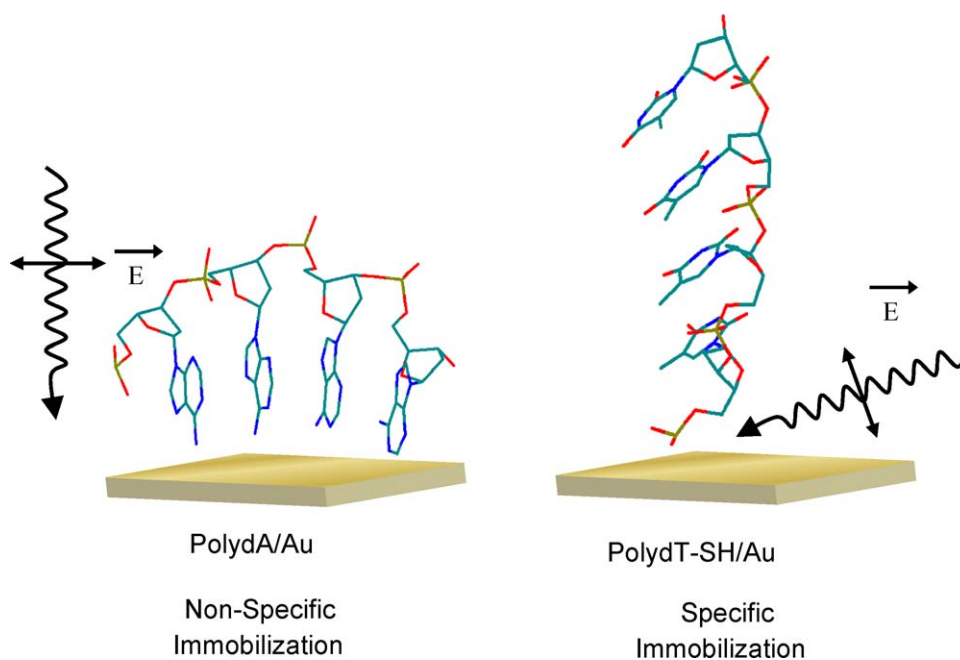


Fig. 8. Idealized schematic indicating the orientation of the polydT-SH and polydA oligomers on gold surfaces. The orientations of the incident X-rays and electric vectors that produce maximum intensity in the  $\pi^*$  region for each ssDNA oligomer are also shown.

[52]. The large change in the  $\sigma^*$  structure between polydA and polydT-SH are consistent with the change between the nitrogen K-edge spectra of adenine and thymine shown in Fig. 2.

#### 4. Conclusions

The major conclusions from the present study are

- NEXAFS spectra at the carbon K, nitrogen K and oxygen K-edges of the DNA nucleobases exhibit a range of features and can be uniquely assigned to specific species in the nucleobases.
- The carbon K and oxygen K-edge NEXAFS spectra show significant differences with the addition of the sugar and phosphate components of DNA. The nitrogen K-edge NEXAFS spectra of adenine and guanine show noticeable shifts in the peak positions of the  $\pi^*$  peaks upon addition of the sugar and phosphate groups.
- Polarization-dependent NEXAFS experiments demonstrate the ability to probe different molecular orientations adopted by polydT-SH and polydA on gold surfaces.

#### Acknowledgements

Financial support from NESAC/BIO (NIH Grant EB-002027) and NIH Grant EB-001473 are gratefully acknowledged. Dr. Zugen Fu is gratefully acknowledged for his help with the experiments and discussion. Members of the NESAC/BIO group are thanked for their helpful discussions and suggestions. The NEXAFS studies were performed at the NSLS, Brookhaven National Laboratory, which is supported by the DOE, Division of Materials Science and Division of Chemical Sciences. Certain commercial names are identified for purposes of example

or clarity; such identification does not indicate endorsement by the National Institute of Standards and Technology.

#### References

- [1] B. Kasemo, Surf. Sci. 500 (1–3) (2002) 656–677.
- [2] M.J. Heller, Annu. Rev. Biomed. Eng. 4 (2002) 129–153.
- [3] S.K. Chanda, J.S. Caldwell, Drug Discovery Today 8 (4) (2003) 168–174.
- [4] J.R. Pollack, T. Sorlie, C.M. Perou, C.A. Rees, S.S. Jeffrey, P.E. Lonning, R. Tibshirani, D. Botstein, A.L. Borresen-Dale, P.O. Brown, Proc. Natl. Acad. Sci. U.S.A. 99 (20) (2002) 12963–12968.
- [5] P. He, Z.Y. Tang, B.B. Liu, S.L. Ye, Y.K. Liu, J. Cancer Res. Clin. Oncol. 125 (2) (1999) 77–82.
- [6] D.G. Wang, J.B. Fan, C.J. Siao, A. Berno, P. Young, R. Sapolsky, G. Ghandour, N. Perkins, E. Winchester, J. Spencer, L. Kruglyak, L. Stein, L. Hsie, T. Topaloglou, E. Hubbell, E. Robinson, M. Mittmann, M.S. Morris, N.P. Shen, D. Kilburn, J. Rioux, C. Nusbaum, S. Rozen, T.J. Hudson, R. Lipshutz, M. Chee, E.S. Lander, Science 280 (5366) (1998) 1077–1082.
- [7] V.G. Cheung, J.P. Gregg, K.J. Gogolin-Ewens, J. Bandong, C.A. Stanley, L. Baker, M.J. Higgins, N.J. Nowak, T.B. Shows, W.J. Ewens, R.S. Spielman, Nat. Genet. 18 (3) (1998) 225–230.
- [8] L. Wodicka, H.L. Dong, M. Mittmann, M.H. Ho, D.J. Lockhart, Nat. Biotechnol. 15 (13) (1997) 1359–1367.
- [9] R.A. Heller, M. Schena, A. Chai, D. Shalon, T. Bedilion, J. Gilmore, D.E. Woolley, R.W. Davis, Proc. Natl. Acad. Sci. U.S.A. 94 (6) (1997) 2150–2155.
- [10] J. DeRisi, L. Penland, P.O. Brown, M.L. Bittner, P.S. Meltzer, M. Ray, Y.D. Chen, Y.A. Su, J.M. Trent, Nat. Genet. 14 (4) (1996) 457–460.
- [11] C.M. Niemeyer, Curr. Opin. Chem. Biol. 4 (6) (2000) 609–618.
- [12] R. Elghanian, J.J. Storhoff, R.C. Mucic, R.L. Letsinger, C.A. Mirkin, Science 277 (5329) (1997) 1078–1081.
- [13] L.A. Chrisey, G.U. Lee, C.E. Offerrall, Nucl. Acids Res. 24 (15) (1996) 3031–3039.
- [14] T.M. Herne, M.J. Tarlov, J. Am. Chem. Soc. 119 (38) (1997) 8916–8920.
- [15] P.L. Dolan, Y. Wu, L.K. Ista, R.L. Metzberg, M.A. Nelson, G.P. Lopez, Nucl. Acids Res. 29 (21) (2001).

- [16] P.T. Charles, G.J. Vora, J.D. Andreadis, A.J. Fortney, C.E. Meador, C.S. Dulcey, D.A. Stenger, *Langmuir* 19 (5) (2003) 1586–1591.
- [17] P. Kumar, J. Choithani, K.C. Gupta, *Nucl. Acids Res.* 32 (10) (2004).
- [18] T. Strother, W. Cai, X.S. Zhao, R.J. Hamers, L.M. Smith, *J. Am. Chem. Soc.* 122 (6) (2000) 1205–1209.
- [19] Y.H. Rogers, P. Jiang-Baucom, Z.J. Huang, V. Bogdanov, S. Anderson, M.T. Boyce-Jacino, *Anal. Biochem.* 266 (1) (1999) 23–30.
- [20] D. Proudnikov, E. Timofeev, A. Mirzabekov, *Anal. Biochem.* 259 (1) (1998) 34–41.
- [21] S.R. Rasmussen, M.R. Larsen, S.E. Rasmussen, *Anal. Biochem.* 198 (1) (1991) 138–142.
- [22] M. Schena, D. Shalon, R.W. Davis, P.O. Brown, *Science* 270 (5235) (1995) 467–470.
- [23] L.K. Wolf, Y. Gao, R.M. Georgiadis, *Langmuir* 20 (8) (2004) 3357–3361.
- [24] H. Kimura-Suda, D.Y. Petrovykh, M.J. Tarlov, L.J. Whitman, *J. Am. Chem. Soc.* 125 (30) (2003) 9014–9015.
- [25] H. Wackerbarth, M. Grubb, J.D. Zhang, A.G. Hansen, J. Ulstrup, *Langmuir* 20 (5) (2004) 1647–1655.
- [26] W.J. Parak, T. Pellegrino, C.M. Micheel, D. Gerion, S.C. Williams, A.P. Alivisatos, *Nano Lett.* 3 (1) (2003) 33–36.
- [27] S.O. Kelley, J.K. Barton, N.M. Jackson, L.D. McPherson, A.B. Potter, E.M. Spain, M.J. Allen, M.G. Hill, *Langmuir* 14 (24) (1998) 6781–6784.
- [28] M.Z. Liu, N.A. Amro, C.S. Chow, G.Y. Liu, *Nano Lett.* 2 (8) (2002) 863–867.
- [29] P.S. Crozier, M.J. Stevens, *J. Chem. Phys.* 118 (8) (2003) 3855–3860.
- [30] D.Y. Petrovykh, H. Kimura-Suda, L.J. Whitman, M.J. Tarlov, *J. Am. Chem. Soc.* 125 (17) (2003) 5219–5226.
- [31] R. Levicky, T.M. Herne, M.J. Tarlov, S.K. Satija, *J. Am. Chem. Soc.* 120 (38) (1998) 9787–9792.
- [32] N. Mourougou-Candoni, C. Naud, F. Thibaudau, *Langmuir* 19 (3) (2003) 682–686.
- [33] S.M. Kirtley, O.C. Mullins, J. Chen, J. Vanelp, S.J. George, C.T. Chen, T. Ohalloran, S.P. Cramer, *Biochim. Biophys. Acta* 1132 (3) (1992) 249–254.
- [34] A. Moewes, J. MacNaughton, R. Wilks, J.S. Lee, S.D. Wettig, H.B. Kraatz, E.Z. Kurmaev, *J. Electron. Spectrosc. Relat. Phenom.* 137–140 (2004) 817–822.
- [35] K. Fujii, K. Akamatsu, Y. Muramatsu, A. Yokoya, *Nucl. Instrum. Meth. Phys. Res. B* 199 (2003) 249–254.
- [36] K. Fujii, K. Akamatsu, A. Yokoya, *J. Phys. Chem. B* 108 (23) (2004) 8031–8035.
- [37] J. MacNaughton, A. Moewes, E.Z. Kurmaev, *J. Phys. Chem. B* 109 (16) (2005) 7749.
- [38] C.J. May, H.E. Canavan, D.G. Castner, *Anal. Chem.* 76 (4) (2004) 1114–1122.
- [39] C.Y. Lee, H.E. Canavan, L.J. Gamble, D.G. Castner, *Langmuir* 21 (11) (2005) 5134–5141.
- [40] J.F. Morar, F.J. Himpsel, G. Hollinger, J.L. Jordon, G. Hughes, F.R. McFeely, *Phys. Rev. B* 33 (2) (1986) 1346–1349.
- [41] N.T. Samuel, D.A. Fischer, D.G. Castner, in preparation.
- [42] V. Carravatta, O. Plashkevych, H. Agren, *J. Chem. Phys.* 109 (4) (1998) 1456–1464.
- [43] O. Dhez, H. Ade, S.G. Urquhart, *J. Electron. Spectrosc. Relat. Phenom.* 128 (1) (2003) 85–96.
- [44] M. Furukawa, H. Fujisawa, S. Katano, H. Ogasawara, Y. Kim, T. Komeda, A. Nilsson, M. Kawai, *Surf. Sci.* 532 (2003) 261–266.
- [45] M.L. Gordon, G. Cooper, C. Morin, T. Araki, C.C. Turci, K. Kaznatcheev, A.P. Hitchcock, *J. Phys. Chem. A* 107 (32) (2003) 6144–6159.
- [46] K. Kaznatcheyev, A. Osanna, C. Jacobsen, O. Plashkevych, O. Vahtras, H. Agren, *J. Phys. Chem. A* 106 (13) (2002) 3153–3168.
- [47] L.G.M. Pettersson, H. Agren, B.L. Schurmann, A. Lippitz, W.E.S. Unger, *Int. J. Quantum Chem.* 63 (3) (1997) 749–765.
- [48] S.G. Urquhart, H. Ade, *J. Phys. Chem. B* 106 (34) (2002) 8531–8538.
- [49] J. Stohr, *NEXAFS Spectroscopy*, Springer-Verlag, Heidelberg, 1992.
- [50] A.G. Shard, J.D. Whittle, A.J. Beck, P.N. Brookes, N.A. Bullett, R.A. Talib, A. Mistry, D. Barton, S.L. McArthur, *J. Phys. Chem. B* 108 (33) (2004) 12472–12480.
- [51] J.R. Lawrence, G.D.W. Swerhone, G.G. Leppard, T. Araki, X. Zhang, M.M. West, A.P. Hitchcock, *Appl. Environ. Microbiol.* 69 (9) (2003) 5543–5554.
- [52] C.-Y. Lee, P. Gong, G.M. Harbers, D.W. Grainger, D.G. Castner, L.J. Gamble, *Anal. Chem.* 78 (2006) 3316–3325.
- [53] J.N. Crain, A. Kirakosian, J.L. Lin, Y.D. Gu, R.R. Shah, N.L. Abbott, F.J. Himpsel, *J. Appl. Phys.* 90 (7) (2001) 3291–3295.
- [54] C. Briones, E. Mateo-Marti, C. Gomez-Navarro, V. Parro, E. Roman, J.A. Martin-Gago, *Phys. Rev. Lett.* 93 (20) (2004).
- [55] D.Y. Petrovykh, V. Perez-Dieste, A. Opdahl, H. Kimura-Suda, J.M. Sullivan, M.J. Tarlov, F.J. Himpsel, L.J. Whitman, *J. Am. Chem. Soc.* 128 (1) (2006) 2–3.